Internal Report
DESY M 96-05
April 1996

Investigation of a Hybrid Coupler for a 6 Meter S-band Linear Collider Accelerating Structure

V. E. Kaljuzhny, D. V. Kostin, S. V. Ivanov,
O. S. Milovanov, N. N. Nechaev, A. N. Parfenov,
N. P. Sobenin, A. A. Zavadzev, S. N. Yarigin

Moscow Engineering Physics Institute MEPhI, Moscow, Russia

M. Dohlus, N. Holtkamp

Deutsches Elektronen-Synchrotron DESY, Hamburg, Germany

Internal Report
DESY M-96-5
April 1996

Investigation of a Hybrid Coupler for a 6 Meter S-band Linear Collider Accelerating Structure

by

V.E.Kaljuzhny, D.V.Kostin, S.V.Ivanov,
O.S.Milovanov, N.N.Nechaev, A.N.Parfenov,
N.P.Sobenin, A.A.Zavadzev, S.N.Yarigin

Moscow Engineering Physics Institute, MEPhI
Kashirskoe shosse , 31, 115409 Moscow, Russia

M.Dohlus, N.Holtkamp

Deutsches Elektronen-Synchrotron, DESY
Notkestrasse 85, 22607 Hamburg, Germany

Contents.

Abstract

The possibility of using the symmetric SBLC coupler for hybrid mode damping is investigated. The requirements for the frequency and Q-factor of the coupler at first dipole mode are obtained on the basis of an equivalent scheme of diskloaded waveguide (DLW) with this coupler. Measurement equipment and methods for investigation of hybrid coupler are considered. The influence of some elements inserted into the coupler cavity to obtain the necessary frequency shift between fundamental and hybrid modes is studied at the experimental prototypes and is calculated with the MAFIA code and with analytical formulas. 30 cells of the first part the SBLC accelerating section were manufactured and used in the experiments to decrease the Q-factor of this structure with coupler in 5 times in some frequency band for both polarization of the first dipole mode. This hybrid coupler may be also used as BPM too.

1.Analysis of hybrid waves damping in SBLC accelerating section.

The analysis of hybrid waves excitation in DESY collider section was carried out on the basis of an equivalent scheme of the disk loaded waveguide (DLW) with HEM_{11} mode. Such a scheme for the DLW cell excited in hybrid mode is shown in Fig.1

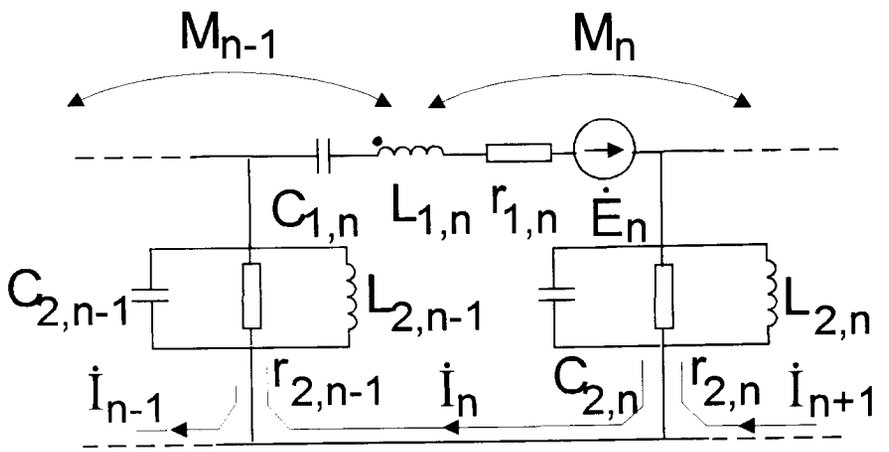

Figure 1 Equivalent scheme of a DLW cell excited in hybrid mode.

In this scheme the series branch (L_{1n} , C_{1n} , r_{1n}) represents the existence of the E_{11} mode electromagnetic field. On the one hand the coupling between cells is realized by magnetic field that is represented in the scheme by mutual inductance M_n . On the other hand there is resonance type coupling by means of H_{11} mode electromagnetic field that is represented by parallel branches (L_{2n} , C_{2n} , r_{2n}). The cell excitation is modeled by introducing complex e.m.f. $\dot{E}_n$ into the series branch. In the scheme under consideration $\dot{I}_n$ are the loop currents complex amplitudes.

It is more convenient to operate with the following parameters expressed in terms of ***L, C, r***

$$f_{1n}=\frac{1}{2\pi\sqrt{L_{1n}C_{1n}}};\qquad f_{2n}=\frac{1}{2\pi\sqrt{L_{2n}C_{2n}}};$$
$$\frac{K_n}{2}=\frac{M_n}{\sqrt{L_{1,n}L_{1,n+1}}};\qquad \frac{K_{12n}}{2}=\frac{\sqrt{C_{1,n}C_{1,n+1}}}{C_{2n}};$$
$$Q_{1n}=\sqrt{\frac{L_{1n}}{C_{1n}}}\frac{1}{r_{1n}};\qquad Q_{2n}=\sqrt{\frac{C_{2n}}{L_{2n}}}r_{2n};\qquad (1)$$
$$\dot{X}_n=\sqrt{L_{1n}}\dot{I}_n;$$

By using these parameters one can obtain the following set of equations with respect to the complex values $\dot{X}_n$

$$\begin{bmatrix} A_1 & B_1 & 0 & . & . & . & 0 \\ B_1 & A_2 & B_2 & . & . & . & 0 \\ . & . & . & . & . & . & . \\ 0 & . & . & . & B_{N-2} & A_{N-1} & B_{N-1} \\ 0 & . & . & . & 0 & B_{N-1} & A_N \end{bmatrix}\begin{bmatrix} \dot{X}_1 \\ \dot{X}_2 \\ \vdots \\ \dot{X}_{N-1} \\ \dot{X}_N \end{bmatrix}=\begin{bmatrix} \frac{\dot{E}_1}{j\omega\sqrt{L_{11}}} \\ \vdots \\ \vdots \\ \vdots \\ \frac{\dot{E}_N}{j\omega\sqrt{L_{1N}}} \end{bmatrix} \qquad (2)$$

where $\omega=2\pi f$ is the section excitation frequency,

$$A_n=1-\frac{f_{1n}^2}{f^2}-j\frac{f_{1n}}{f}\frac{1}{Q_{1n}}-\frac{f_{1n}^2}{f^2}\left[\sqrt{\frac{C_{1n}}{C_{1,n-1}}}\frac{K_{12,n-1}}{2}\frac{1}{1-\frac{f_{2n-1}^2}{f^2}-j\frac{f_{2,n-1}}{f}\frac{1}{Q_{2,n-1}}}+\right.$$
$$\left.+\sqrt{\frac{C_{1n}}{C_{1,n+1}}}\frac{K_{12,n}}{2}\frac{1}{1-\frac{f_{2n}^2}{f^2}-j\frac{f_{2,n}}{f}\frac{1}{Q_{2,n}}}\right]; \qquad (3)$$

$$B_n=\frac{K_n}{2}+\frac{K_{12,n}}{2}\frac{f_{1,n}f_{1,n+1}}{f^2}\frac{1}{1-\frac{f_{2,n}^2}{f^2}-j\frac{f_{2,n}}{f}\frac{1}{Q_{2,n}}}. \qquad (4)$$

At n=1 the multiplier $\sqrt{\frac{C_{1n}}{C_{1,n-1}}}\frac{K_{12,n-1}}{2}$ in A_1 should be changed by $\frac{K_{12,0}}{2}=\frac{C_{1,1}}{C_{2,0}}$, whereas at n=N the multiplier $\sqrt{\frac{C_{1N}}{C_{1,N+1}}}\frac{K_{12,N}}{2}$ should be changed by $\frac{K_{12,N}}{2}=\frac{C_{1,N}}{C_{2,N}}$.

Note that in the equivalent circuit the number of parallel branches is equal to N+1 , whereas there are N series branches , where N is the number of cells in the section . The first and the last parallel branches (indexes 0 and N) are introduced for modeling beam pipe in the input and output couplers.

Voltages across the capacitive element C_{1n} ($\dot{U}_{z,n}$) and C_{2n} ($\dot{U}_{r,n}$) are related to $\dot{X}_n$ by the following expressions :

$$\dot{U}_{z,n}=-j\frac{f_{1,n}}{f}\frac{\dot{X}_n}{\sqrt{C_{1,n}}}\ ,\ (n=1,2,\ldots,N) \qquad (5)$$

$$\dot{U}_{r,n} = \frac{K_{12,n}}{2} \frac{1}{1 - \frac{f_{2,n}^2}{f^2} - j\frac{f_{2,n}}{f}\frac{1}{Q_{2,n}}} \left(\sqrt{\frac{C_{1,n}}{C_{1,n+1}}} \dot{U}_{z,n} - \sqrt{\frac{C_{1,n+1}}{C_{1,n}}} \dot{U}_{z,n+1} \right), \tag{6}$$

(n = 1,2,..., N - 1)

$$\dot{U}_{r,0} = -\frac{K_{12,0}}{2} \frac{1}{1 - \frac{f_{2.0}^2}{f^2} - j\frac{f_{2.0}}{f}\frac{1}{Q_{2.0}}} \dot{U}_{z,1} \tag{7}$$

$$\dot{U}_{r,N} = \frac{K_{12,N}}{2} \frac{1}{1 - \frac{f_{2,N}^2}{f^2} - j\frac{f_{2,N}}{f}\frac{1}{Q_{2,N}}} \dot{U}_{z,N} \tag{8}$$

By using the equivalent scheme one can obtain the dispersion relation for the infinite uniform lossless DLW ($f_{1,n}=f_1$, $f_{2,n}=f_2$, $\boldsymbol{K}_n=\boldsymbol{K}$, $\boldsymbol{K}_{12,n}=\boldsymbol{K}_{12}$, $\boldsymbol{Q}_{1,n}=\infty$, $\boldsymbol{Q}_{2,n}=\infty$) in the following form

$$f = \sqrt{\frac{F(\varphi) \pm \sqrt{F^2(\varphi) - 4f_1^2 f_2^2 (1 + K\cos\varphi)}}{2(1 + K\cos\varphi)}} \ , \tag{9}$$

where $F(\varphi) = f_1^2\left[1 + K_{12}(1 - \cos\varphi)\right] + f_2^2(1 + K\cos\varphi)$, φ is the phase shift per DLW cell, f is the frequency corresponding to φ .

The upper sign in (9) corresponds to the higher branch of the dispersion relation whereas the lower one corresponds to the lower branch.

If we denote f_{01} and $f_{\pi 1}$ as the frequencies of the 0 and π modes of the lower branch and f_{02} and $f_{\pi 2}$ as similar values for the upper branch of the dispersion curve we can write down the following expressions for f_1 , f_2 , $\boldsymbol{K}$, $\boldsymbol{K}_{12}$:

$$f_1 = f_{01}\sqrt{1 + K} \quad , \quad f_2 = f_{02} \tag{10}$$

$$\text{or } f_1 = f_{02}\sqrt{1 + K} \quad , \quad f_2 = f_{01} \tag{10'}$$

$$K = \frac{(f_{\pi 1} f_{\pi 2})^2 - (f_{01} f_{02})^2}{(f_{\pi 1} f_{\pi 2})^2 + (f_{01} f_{02})^2} = \frac{2M}{L_1} \tag{11}$$

$$K_{12} = \frac{1}{2}\left[(1 - K)\frac{f_{\pi 1}^2 + f_{\pi 2}^2 - f_2^2}{f_1^2} - 1 \right] = \frac{2C_1}{C_2} \tag{12}$$

The frequencies f_{01} and f_{02} are correspondingly linked to the field distributions as shown in Fig.2 a,b :

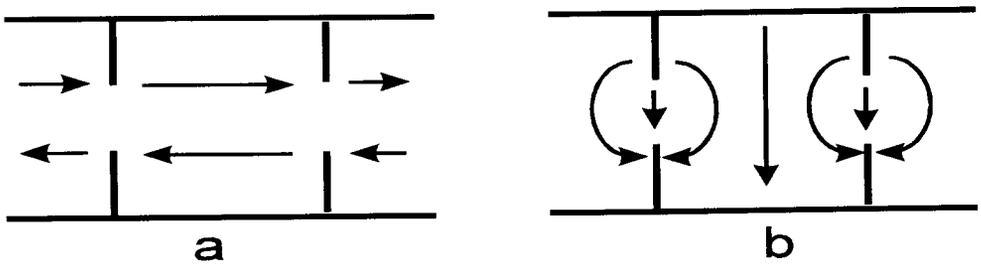

Figure 2. Electric field in DLW corresponding to 0 mode.

The frequencies $f_{\pi 1}$ and $f_{\pi 2}$ are correspondingly linked to the field distribution as shown in.Fig 3. Occasionally the frequencies corresponding to the field distribution shown in Fig. 2 a and Fig. 2b is denoted as f_{0E} and f_{0H}. The symbols E and H indicate at electric and magnetic waves. The frequencies f_{0E} and f_{0H} may be excited in the DLW cells using electric or magnetic walls in the middle of disks. Therefore these frequencies may be denoted as f_{EW0} and f_{MW0}. Correspondingly the frequencies $f_{\pi 1}$ and $f_{\pi 2}$ can be denoted as $f_{MW\pi}$ and $f_{EW\pi}$. Depending on DLW dimensions may be $f_{EW0} > f_{MW0}$ or $f_{EW0} < f_{MW0}$, but always

$f_{EW\pi} > f_{MW\pi}$.

In accordance with this formula (10) can be rewritten in more common form

$$f_1 = f_{EW0}\sqrt{1+K}\ ,\ f_2 = f_{MW0} \qquad (13)$$

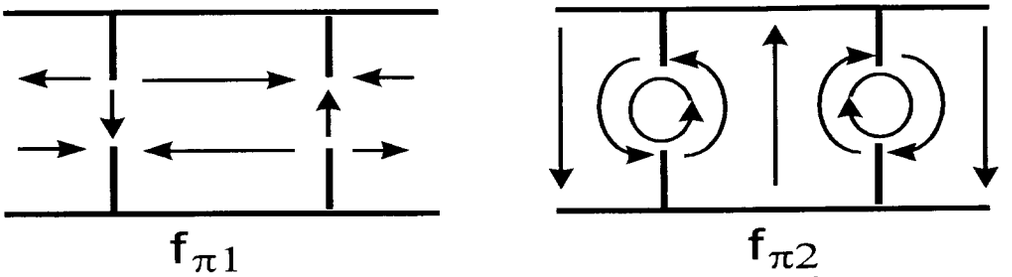

Figure 3. Electric field in DLW corresponding to π .mode.

The dependencies of the frequencies $f_{MW\pi}, f_{EW0}, f_{MW0}, f_{EW\pi}$ on the cell number for SBLC accelerating section are shown in Fig. 4. The disk aperture radius is varied from 15.34mm to 11.003mm. The inner radius of the cells was changed in such a way that the operational frequency of $2\pi/3$ mode was 2998 MHz..

The modeling of the input coupler was realized by means of changing the parameters $f_{11}= f_{1C}$ and $Q_{11}= Q_{1C}$ of the first cell series branch in such a way that we would have a traveling wave regime in the DLW consisting of cells similar to the first one, the operational frequency of the traveling wave regime being f_{op} , the phase shift per a cell at this frequency being φ_{op} .

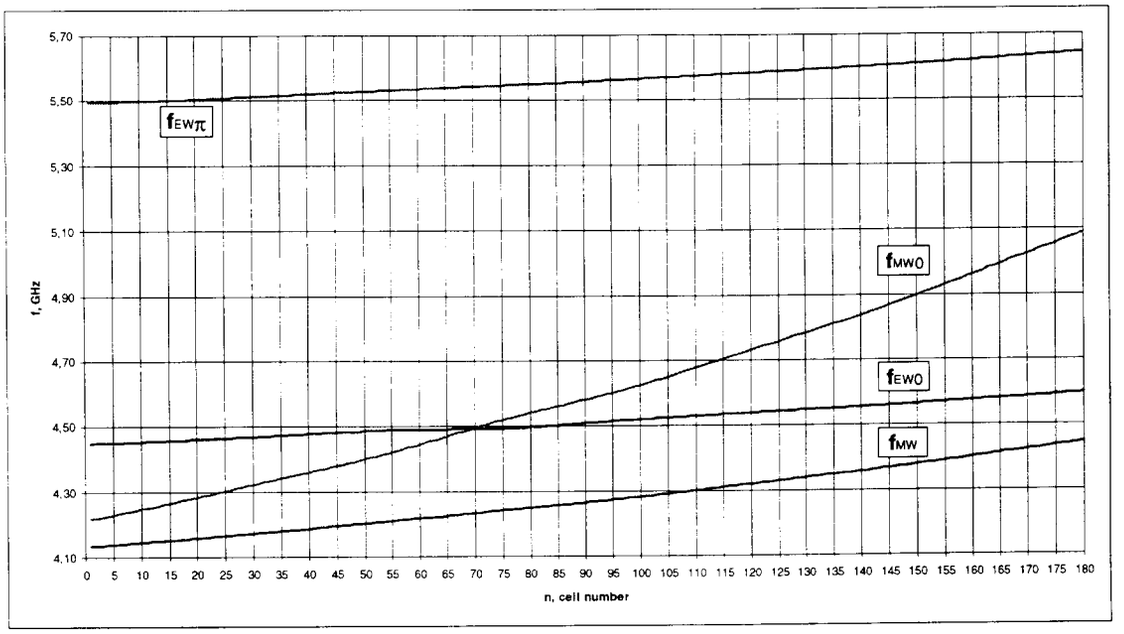

Figure 4. Dependence cut off frequencies versus cell number for SBLC accelerating section.

Using equations (2), (3), (4) values U_z were calculated as a function of the cell number at different frequencies for the SBLC accelerating section with constant gradient , consisting of the first 30 cells (see Fig. 5.). Curves 1 in these pictures correspond the case when the input coupler is mismatched with the first accelerating section cell . Curves 2 correspond the case when input coupler is matched with DLW at the frequency f_{op} =4.151MGz ($\varphi_{op}=95^0$).

Excitation of the accelerating section has been simulated by introduction of e.m.f. into the cells 2, 8, 13 and 18 at the frequencies 4.13760 GHz , 4.14495 GHz, 4.15096 GHz and 4.15908 GHz correspondingly. At these frequencies similar patterns were obtained using the perturbation method for the first 30 cells of the mismatched input coupler (see Fig. 12). These data are included in the next chapter. In all the calculations the series branch resonant frequency f_{11} was chosen 4.846777 GHz and with the Q-factor Q_{11} of 14.677. These values correspond to the lowest resonant frequency of the coupler cell f_c=4.152224 GHz and Q-factor Q_c=159.77.

From Fig. 5 one may see that the matching of the coupler at the hybrid mode reduces the amplitude of electric field more than five times in a broad frequency band. The analogous results for DLW with constant gradient but without a coupler were obtained in work / 1 /.

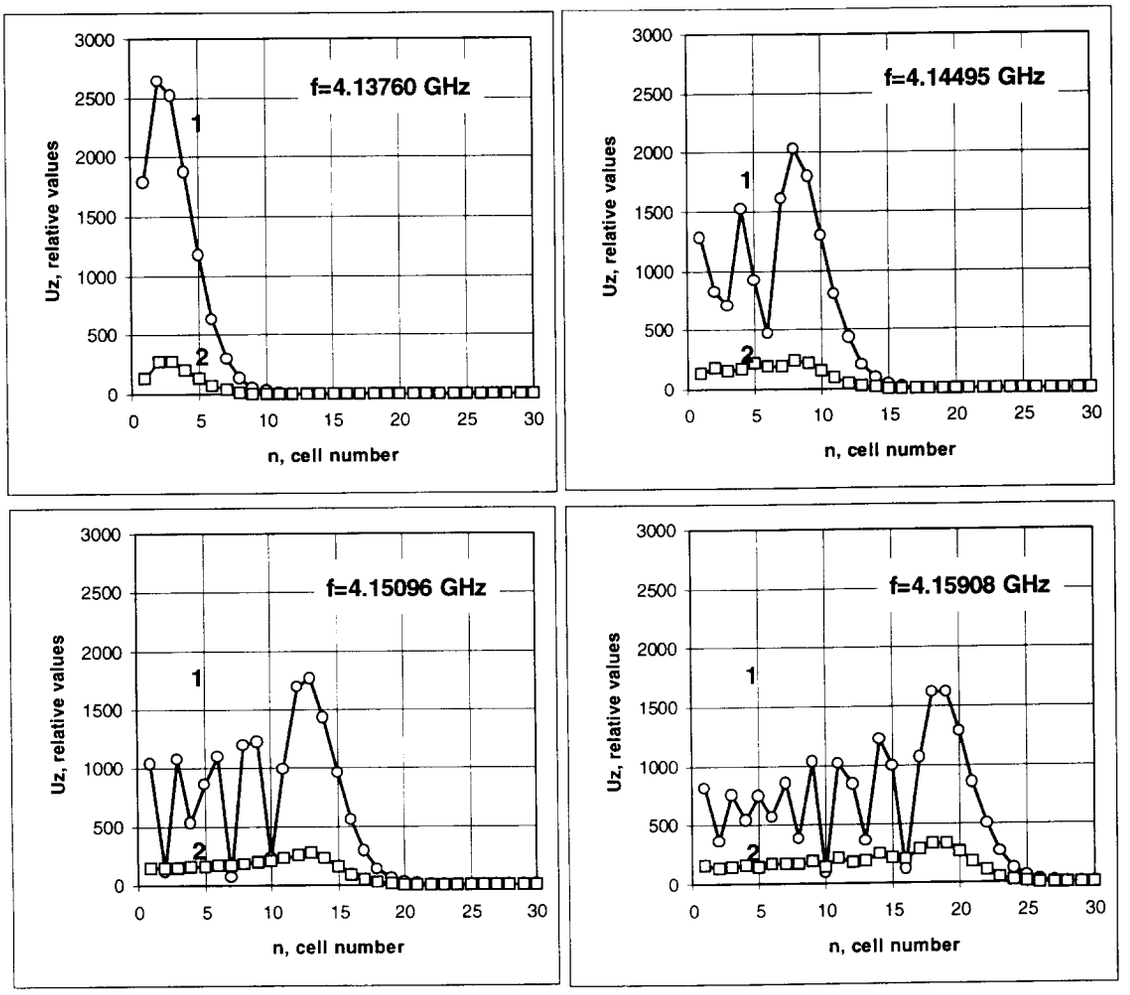

Figure 5. Values U_z versus cell number for the first 30 cells of SBLC DLW at different frequencies. Curves 1 correspond mismatched input coupler; curves 2 correspond matched input coupler.

2. Measurement equipment and methods of hybrid coupler investigation.

The basic idea of hybrid mode damping using the existing symmetric coupler is that ,by choosing the impedance introduced into the coupler from the incoming rectangular waveguides, the matching between the coupler and DLW at hybrid wave frequencies can be provided. Naturally the matching at the operational frequency should be maintained. To obtain such a matching regime at two frequencies the following modifications had to be introduced into the coupler construction / 2 /. Since the T-junction at hybrid wave frequencies is similar to the short circuit and the length l_1 variation of the ports parallel to the coupler (length $l_1$between T-junction and coupler) does not lead to the mismatching at the operational frequency. Thus we can change the impedance introduced into the coupler in the hybrid mode simply by varying this length l_1. To dissipate the hybrid wave which is withdrawn into rectangular guides the absorbing loads should be used instead of short-circuiting planes. The absorbing loads are made on the basis of rectangular waveguides providing a cut-off regime for the operational mode. The impedance value that is introduced into the coupler by these loads should be determined by means of hybrid wave power transmission coefficient measurements or Q-factor measurements. It is apparent that in the process of such measurements we can determine reflection coefficients from absorbing loads as well as l_1 and l_2 (length l_2 between coupler and absorbing loads) required for the coupler and DLW to be matched in the hybrid wave.

All measurements described below were carried out with the coupler dimensions which corresponded to those of the first version SBLC DLW first cell (2a=31.02mm, 2b=82.81mm, D=33.3mm, t=5mm). Since the loss coefficient in the lower branch of the HOM mode dispersion curve is much higher than that in the upper one our measurements were limited by the frequencies of the lower branch (frequencies from 4.120 GHz to 4.190 GHz, when the measurements were carried out at the DLW with constant impedance with 2a=31.02mm and frequencies from 4.13 GHz to 4.185 GHz and more in the case with first 30 cells of SBLC DLW) .

.During the investigations of the hybrid coupler some methods were used to evaluate the damping effect. Fig 6. shows one scheme for measuring the electric field longitudinal component distribution along the DLW SBLC at frequencies of the first dipole mode. An accelerating structure to be studied is included into the feedback loop of the complex amplifier by means of two coupling elements (2 and 3), which are inserted into DLW cells through holes in the side walls. The measuring instrumentation (12) can be used for determination of frequency shifts (by means of the movement of perturbing bodies (13)) in the range from 2.5 to 7 GHz . The movement of perturbing bodies is synchronized with the resonant frequency shift display. The operational stability of the instrumentation, as well as the frequency shift measurement accuracy, depend on the Q-factor of the structure under investigation. Values of Q-factor in our measurements have been varied from 1500 to 10000 which provided conditions for successful operation of the instrumentation. Metal cylinders with length 12 mm and diameter 0.1 mm were used as perturbing bodies. They were moved along the structure at a distance of 6 mm from the axis in the wave polarization plane.

The coupler (4) was attached to the opposite end of the DLW and was connected with rectangular waveguides (5). Their cross-section dimensions are $72\times28.3mm^2$. One side of the waveguides were terminated by movable short circuit plungers(10), on the other side absorbing elements (receivers) for the hybrid wave were connected. The receivers consisted of the waveguide transition (5) from $72\times28.3mm^2$ to $48\times24mm^2$ cross-section, the $48\times24mm^2$ waveguide section (9) with adjustable pins, the receiving probe (7) and the matched dissipative load (6). By adjusting the extension of pins (8)inserted into the waveguide in different combinations (we had 8 pins placed over one half wave length) it is possible to vary the reflection coefficient amplitude and phase, i.e. the impedance value transformed into the coupler.

It is required that damping should be effective for both mode polarization. For this purpose two additional coupling holes between the coupler cavity and the rectangular waveguides with $48\times24mm^2$ cross-section dimensions were cut, the holes being situated diametrically opposite each other. In addition these holes were displaced by 90^o with respect to the existing holes . As in the previous case, the rectangular waveguide network consisted of pin-type matching transformers(8), pin-type receiving elements(7) and absorbing devices(6) .

We used two other schemes , which differed from that shown in Fig. 6 by exciting and receiving setups. In one of them the DLW was excited by a loop, the dimensions of which were chosen in such a way that at frequencies in the middle of the lower dispersion branch of the HOM mode, the coupling was critical. The additional fine tuning when the frequency is changed, was realized by means of sliding short-circuiting plungers inserted into the DLW. RF generator power was fed through the reflectometer , which enables the complex values of the reflection coefficient to be determined.

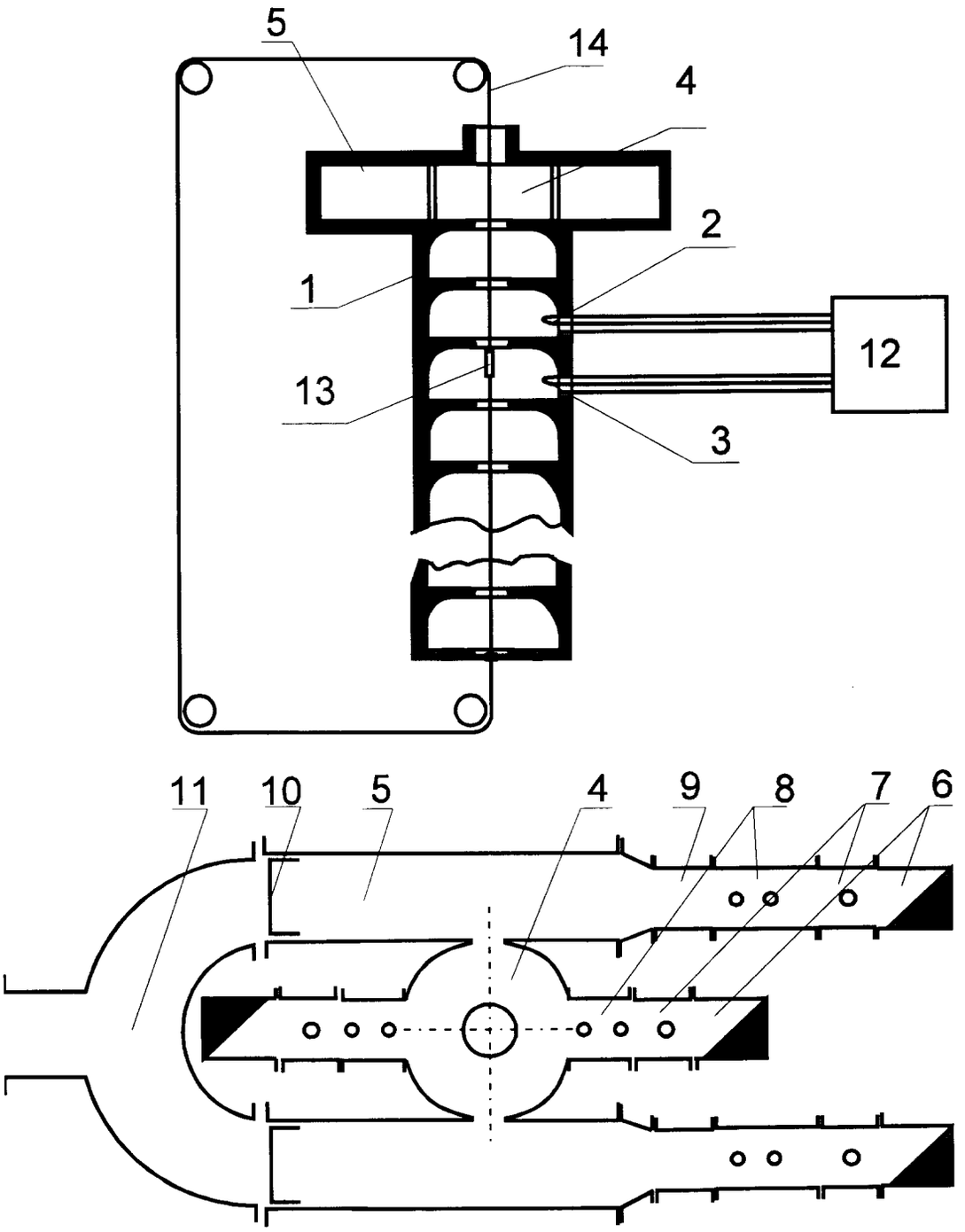

Fig.6. : Scheme of the measurement equipment for the determination of longitudinal electric field distribution along the structure.

The matching of the loop coupling elements with the DLW was realized by means of an iconocenter method in which reflection coefficients from the load were measured when it was moved along the waveguide. By changing the dimensions of the coupling loop and the tuning plunger matching at the input was obtained that was characterized by $\Gamma_{in} < 0.05$.

Note that rotation of the cell with the loop coupling element ,with respect to other elements of the structure, leads to the change of HOM polarization in the DLW. In our case, the loop azimuthal position is chosen in such a way that maximal field amplitude at HOM frequencies is excited in the coupler ports due to the corresponding position of the polarization plane.

The receiving element has been calibrated before conducting the measurements. The calibration process was as follows. First dissipative wedges of the loads are chosen so that $\Gamma \leq 0.01$ over the whole frequency band for the lower branch of the hybrid mode dispersion curve. Then dimensions of the receiver short circuit cross section were determined at the operational frequency 2998 MHz and by means of additional planes they were made such that the coupler matching at the operational frequency was restored. Further the calibration of the probe was carried out, i.e. its position was chosen so that the

signal level withdrawn from the probe should be equal to the incident wave signal level which is applied to the DLW input. Finally, the input impedance characteristic of the receiving element when the positions of the reactive pin insertions were varied was measured. In the process of the measurements, the shape and the surface resistance of the dissipative load were chosen to ensure correct determination of the iconocenter at the different frequencies. The reflection coefficient does not exceed $|\Gamma| = 0.05$ (according to the iconocenter position).

After conclusion of all preparatory studies the prototype structure was tuned for obtaining maximum power transmission coefficient at the hybrid mode frequency. The power transmission coefficient here is defined as

$$K_t = |S_{21}|^2 = \frac{P_{out}}{P_{in}},$$

Note that the receiving devices (7) at the outputs were calibrated at every frequency with respect to the incident wave at the reflectometer and $|U_1| = |U_2|$.

Instead of the transfer coefficient measurement method, the measurements of the loaded Q-factor of the DLW together with the coupler and the coupling channels were performed. The change of the method was caused by the fact that measurements of the transfer coefficients were tiresome and not sensitive in the vicinity of the transfer coefficient value equal to 1 where the absorbing effect is most apparent. According to this technique the Q_l measurement consisted in exciting the desired type of wave by means of a loop (or pin) probe and subsequently withdrawing the signal out of the resonant system and applying it to a receiving device. Measurements were carried out with different numbers of DLW cells taken from the available set of 30 cells. The Q-factor of the system with both polarization's of the hybrid wave were measured.

3. An approach to the tuning of the coupler at the hybrid mode.

It is apparent that to find a method of coupler tuning to the required hybrid mode frequency, while maintaining the tuning at the fundamental mode, we have to study the influence of some elements inserted inside the coupler cavity on the change of the hybrid mode field pattern , i.e. on the values of corresponding frequencies. The problem of conducting the correct electrodynamic calculation of such a complicated system as the coupler cavity with discontinuities, connected to four rectangular waveguides and DLW is rather complex. So the problem is to be solved by combining calculations of structures and experiments on prototypes. The starting point for our studies was the fact that the difference between the coupler frequencies at the fundamental and hybrid modes should be in the range 1150-1230 MHz. It is indeed so because the coupler cavity resonant frequency at the fundamental mode is equal to 2980 MHz (it was determined experimentally) whereas, at the hybrid mode, it should be inside the pass-band of the first cell of DLW, i.e. between 4130 and 4215 MHz .

The choke type groove and circular protrusion (Fig.7) were considered as discontinuities to be inserted into the coupler cavity. The calculation results for the version with the choke-type groove has been realized but calculation as well as experimental investigation have shown that it was rather difficult to analyze the field pattern due to the presence of multiple intercombined modes. These modes were apparently related to cylindrical and coaxial cavities. So the distinct identification of frequency shifts of the cylindrical resonator with modes closely corresponding to E_{010} and E_{110} was hardly possible.

Cavity versions without rectangular guides are shown in Fig 7. They were calculated by means of computer programs SUPERFISH, PRUD-0 as well as URMEL and MAFIA. The calculations were carried out for the axially symmetrical modes (the lowest of them is denoted as E_{010}) as well as for axially non-symmetrical modes, primarily for modes close to E_{110}. The circular protrusion with the height h_1, width Δr_1 and inner radius $\left(r_1 - \frac{\Delta r_1}{2}\right)$ was attached to the coupler cavity butt-end. The resonant frequencies of a cylindrical cavity with modes mentioned above were calculated. The cavity

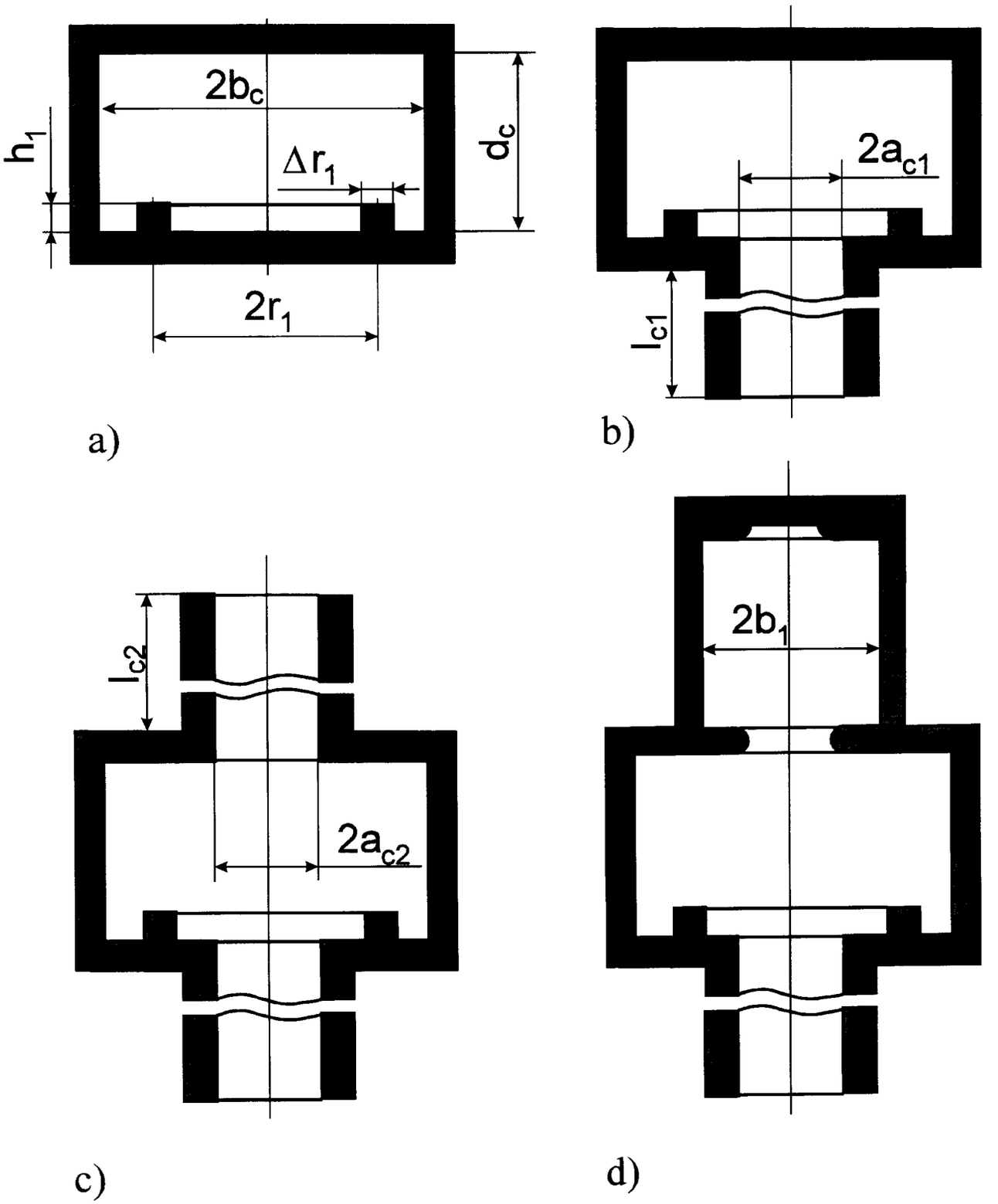

Fig.7. Cylindrical resonator with ring-type protrusion (a), with one drift tube (b), with two drift tubes (c), with detuned first cell (d).

dimensions were: d_c=28.33 mm and $2b_c$ variable. Also the resonators shown in Fig 7a, b, c, d were analyzed. The beam aperture diameter $2a_c$ was chosen to be 31.02 mm and the resonator length $l_c \approx 100$ mm. The difference between Fig .7.d and Fig 7.c is that instead of one drift tube a detuned first cell of DLW ($2b_1$=40 mm) with middle plane short-circuit disk is used

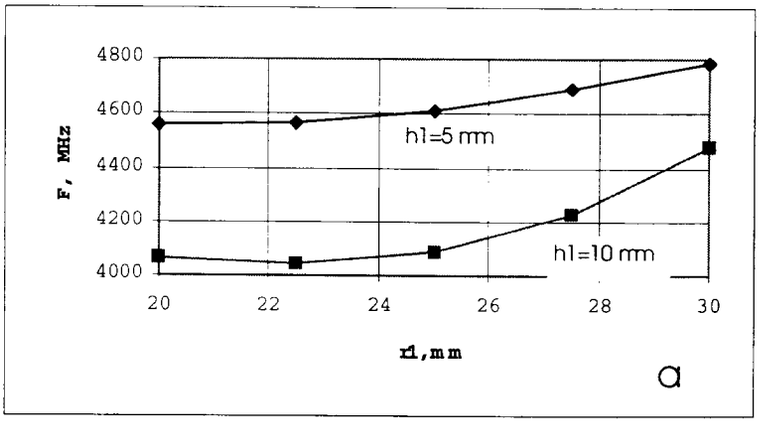

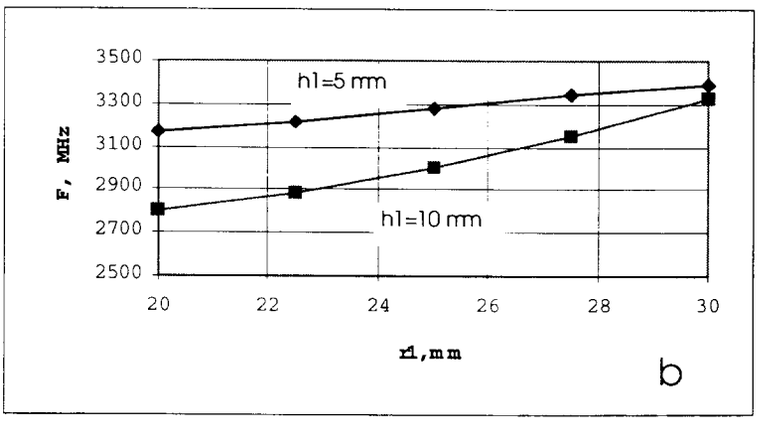

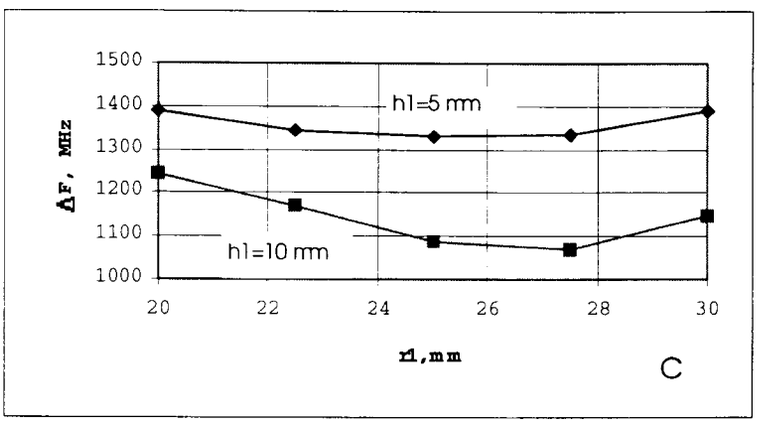

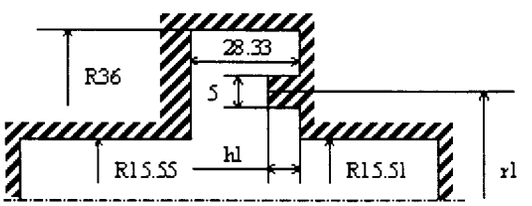

Fig. 8.Frequencies versus dimensions r1 and h1 of the coupler with ring-type protrusion for E_{110} mode (a), E_{010} mode (b) and difference between these frequencies (c).

Some calculation results for the frequencies of the resonator with a circular protrusion and two drift tubes, operating at the mode close to $\mathbf{E_{010}}$ and $\mathbf{E_{110}}$, can be seen in Fig 8. The frequency difference between these two cases varies as shown in the same Fig.8. Calculations were carried out for resonators with values $\mathbf{2b_c}$=72mm and the fixed values of $_{12}\mathbf{d_c}$=28.33 mm.

The average radius of the protrusion, r_1 ,and its height were chosen as variable parameters. The protrusion width was equal to 5 mm. Similar computations were conducted for resonators which, apart from circular protrusions, had additional grooves in the drift tubes. However those calculations gave no positive results. Measurements carried out with prototypes shown in Fig 7.a, b, c and having dimensions $\mathbf{2b_c}$=68mm, 70mm and 72mm demonstrated that calculation results differed from that of measurements in the limits 0.5-1%. If one of the drift tubes is replaced by the detuned first cell (its diameter is diminished to 40mm) the $\mathbf{E_{110}}$ -mode frequency change is not large. At $\mathbf{2b_c}$=70mm and $\mathbf{h_1}$=0 it decreased by 11MHz.

The method of resonator-analog was used to estimate the influence of slots, connecting rectangular waveguides with the coupler, on the coupler resonant frequency / 3 /. This method also permits the coupling coefficient between the coupler cavity and the rectangular guides to be estimated. It is of importance in solving the problem under consideration. According to this method the normalized input impedance of a prismatic resonator with H_{10p}- modes, which is connected to the rectangular waveguide by means of an inductive iris, can be written as

$$Z_{in} = \frac{2Q_r}{\pi p}\left(\frac{\lambda}{\lambda_W}\right)\cdot\left(\frac{A}{\lambda_W}\right)^2 \mathrm{tg}^4\left[\frac{\pi(2a-t)}{2A}\right], \qquad (13)$$

where A and B are dimensions of the broad and narrow walls of the rectangular waveguide, $2a$ and t are the coupling slot width and depth, λ and λ_W are the wave length in the free space and in the waveguide, Q_r is the quality factor of the resonator. It is assumed that Z_{in} would not change with replacement of the prismatic resonator by the resonator to be studied if tangential components at the coupling slot were equal. Limiting the analysis only to the fundamental mode (in our case it is E_{110}) one can write this requirement as

$$\frac{H_r^2}{P} = \frac{H_a^2}{P},$$

where: H_r-from the side of the prismatic resonator,

H_a-from the side of the resonator-analog

P- the power of losses in the resonators.

Now (13) can be rewritten as:

$$Z_{in} = \frac{H_a^2}{P}\frac{Z_0 AB}{4}\cdot\left(\frac{A}{\lambda_W}\right)^2 \mathrm{tg}^4\left[\frac{\pi(2a-t)}{2A}\right], \qquad (14)$$

The ratio $\frac{H_a^2}{P}$ can be determined by any of the known methods.

The coupler frequency shift due to the coupling slots is calculated by the formulae:

$$\frac{\Delta f}{f} = -\frac{ABZ_0\lambda_W}{32\pi c}\frac{H_a^2}{W_a}\mathrm{arctg}\left\{\frac{2A}{\lambda_W}\mathrm{tg}^2\left[\frac{\pi(2a-t)}{2A}\right]\right\}, \qquad (15)$$

where W_a is the energy stored in the resonator-analog.

The frequency shift and coupling coefficient calculations according to (14) and (15) were carried out initially for the coupler connected with the drift tube instead of DLW. As an illustration the corresponding data for the coupler without the circular protrusion (h=0) and with the protrusion of varying height (h=4,6,8mm) and width 5mm and average radius 25mm are presented in Fig.9. On the basis of Fig.9. and Fig.10 one can determine the resonant frequency shifts of the coupler due to the coupling slots of the coupler cell with rectangular waveguide 1 (WG1) and waveguaide 2 (WG2). (see Fig.11). Calculated values of resonant frequency, Q-factor and ratio H^2/W for the structure, shown in Fig.7c, are presented in Table1. This data is used in formula (2.1) and (2.2). In Table 1. one can also see the derivative of the E_{110} mode frequency with respect to the protrusion height for two values of the coupler cavity diameter. Also the derivative of that frequency with respect to the $2b_c$ dimension is presented.

Table 1.. Electrodynamic parameters of the structure in Fig.7.c
with the following dimensions :
d_c=28.33 mm , $2a_{c1}$=31.02 mm , $2a_{c2}$=31.10 mm ,
$l_{c1}=l_{c2}$=100 mm , r_1=25 mm , Δr_1=5 mm .

$2b_c$, mm	h_1, mm	f, MHz	Q	H^2/W, $\times 10^{10}$ $A^2/(J\cdot m^2)$	$\partial f/\partial h$, MHz/mm	$\partial f/\partial 2b_c$, MHz/mm
70	0	4928.7	16280	2.6408	-17.5	-63.5
	2	4893.4	15420	3.2918	-50.6	-63.0
	4	4792.6	13860	3.6940	-74.6	-61.0
	6	4643.3	11840	5.6102	-105	-52.0
	8	4433.5	10030	7.4635	--	-48.0
72	0	4801.7	15790	2.6505	-17.4	--
	2	4767.0	15490	2.7987	-40.5	--
	4	4670.5	14170	3.5186	-65.8	--
	6	4539.0	12390	4.7866	-101	--
	8	4337.9	10760	6.0524	--	--

The data can be used only for approximate calculations of the coupling slot width and depth ($2a_1$, t_1 for WG1 and $2a_2$, t_2 for WG2 in Fig.11.), because relationships for the calculations were deduced with some serious assumptions. Thus, the use of maximal field value over all slot surface in the ratio H^2/W leads to the considerable error. Nevertheless, experiments with prototypes have shown that approximation accuracy is sufficient for the coupler design. So in our experiments with prototypes we have used couplers with the dimensions and the calculated values of χ_1 , χ_2, , Δf_1 and Δf_2 given in Table 2.

For the structure showed at Fig.7c the frequencies of the dipole mode were calculated using the MAFIA code. Similar calculations were carried out for the fundamental mode E_{010}. The results for one of the prototypes are presented in Table 2. The values of the resonant frequency at h_1=0 and h_1=6mm without feeding waveguides were 3356.5MHz , those of the Q-factors were 14180 and 10350, the parameter H^2/W was equal to 1.585 $x10^{10}$ and 2.263$x10^{10}$ $A^2/(m^2J)$ respectively. The coupling slots in the waveguides WG1 resulted in a frequency change of 161MHz at h_1=0 and 233MHz at h_1=6mm. Similar values for the WG2 were 27.3 and 33.7MHz The final calculated frequency values for E_{010}-mode together with experimental ones are presented in Table 2.

Now we consider the system in which the upper wall with the drift tube is replaced by 30 initial cells of DLW SBLC. A priori it is clear that for such a system the values of the coupling coefficient between the cavity and feeding waveguides WG1 and WG2 as well as the change in the hybrid wave frequency would be smaller. The drop would be greater for higher frequencies of the hybrid mode (more cells filled with RF power).

The calculations of the frequency shift and coupling coefficient according to (14) and (15)(for 30 cells of DLW SBLC with the coupler) were carried out for the frequencies which were chosen for preliminary measurements of the electric field longitudinal component distribution along the structure.The measurements were conducted with the cylindrical perturbing body with dimensions 10x1 mm^2. The cylinder was moved along the structure at a distance of 6mm from the axis. The structure with the coupler was tuned to the operational frequency, so it was detuned from the first dipole mode frequencies. The corresponding results are shown in Fig.12. The field distributions at different frequencies were helpful in the estimation of the effective number of cells p which should be taken into account in calculations of the frequency shift and coupling coefficient according to (14) and (15). Assuming the field in the coupler is the same as in the first cell and the stored energy in the every cell is equal, let us define the effective number of cells as

$$p = \frac{\sum_{0}^{30} E_i^2}{E_0^2} \qquad (16)$$

Table 2. Coupling coefficients and resonant frequencies of the coupler prototypes.

h_1, mm. (r_1=25mm, Δr_1=5mm)	parame-ters	$2b_c$=70.0mm $2a_1$=36.4mm t_1=11.0mm $2a_2$=20.0mm t_2=4.0mm E_{110} calculated	$2b_c$=71.9mm, $2a_1$=34.8mm, t_1=10.0mm, $2a_2$=15.0mm, t_2=3.0mm.			
			E_{110}		E_{010}	
			calculated	experi-mental	calculated	experi-mental
0	χ_1	260	220	--	--	--
	χ_2	62	18	--	--	--
	Δf_1, MHz	-380	-350	--	--	--
	Δf_2, MHz	-130	-64	--	--	--
	f_1, MHz	4548	4460	4416	3168	3124
	f_2, MHz	4798	4746	4704	--	--
6	χ_1	395	305	--	--	--
	χ_2	90	23	--	--	--
	Δf_1, MHz	-770	-615	--	--	--
	Δf_2, MHz	-270	-110	--	--	--
	f_1, MHz	3873	3930	3895	2981	2958
	f_2, MHz	4373	4435	4405	--	--

As a result we have the relation between the hybrid mode frequency and number p which is presented in Table 3.

The ratio $(H_a)^2/Wa$ calculated by means of the URMEL program were taken from Table 1. Two cases of coupling were analyzed. In the first two rectangular waveguides (WG1) with dimensions A_1 =72 mm and B_1=28.3 mm were connected to the coupler cavity through the narrow wall and parallel to each other. In the second one two rectangular waveguides with cross-section dimensions A2 =48 mm and B_2=24 mm were connected to the coupler cavity by their butt-ends and opposite to each other (WG2).

Table 3. Effective number of cells at the frequency of hybrid mode.

f, GHz	p
4.13008	9
4.13395	11
4.13654	18
4.13932	22
4.14406	20
4.14700	20
4.14980	37

To determine the frequency shift of the coupler together with the section at definite frequencies, one has to divide the shift by the effective number of cells, corresponding to those frequencies.It is clear that the coupling slots dimensions for the waveguides WG1 and WG2, which are presented in Table 2, can not provide the same change of the coupler frequency and the coupling coefficient at the hybrid mode.

A similar conclusion follows from the calculations of the system including 30 cells of DLW.

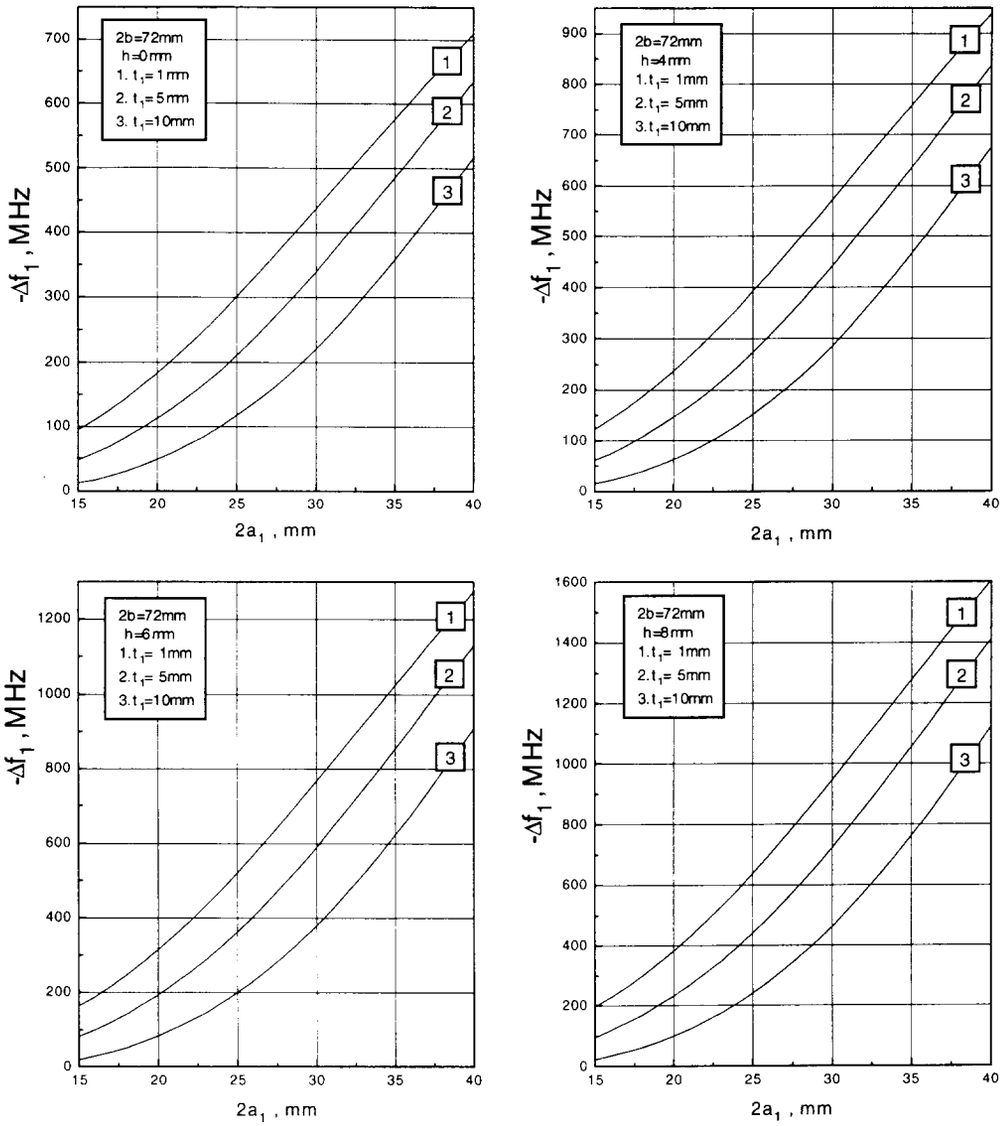

Fig. 9. Frequency shift of coupler cell caused by of two coupling
windows of WG1 with coupler cell
with two drift tubes and round-type protrusion height h (fig.11)

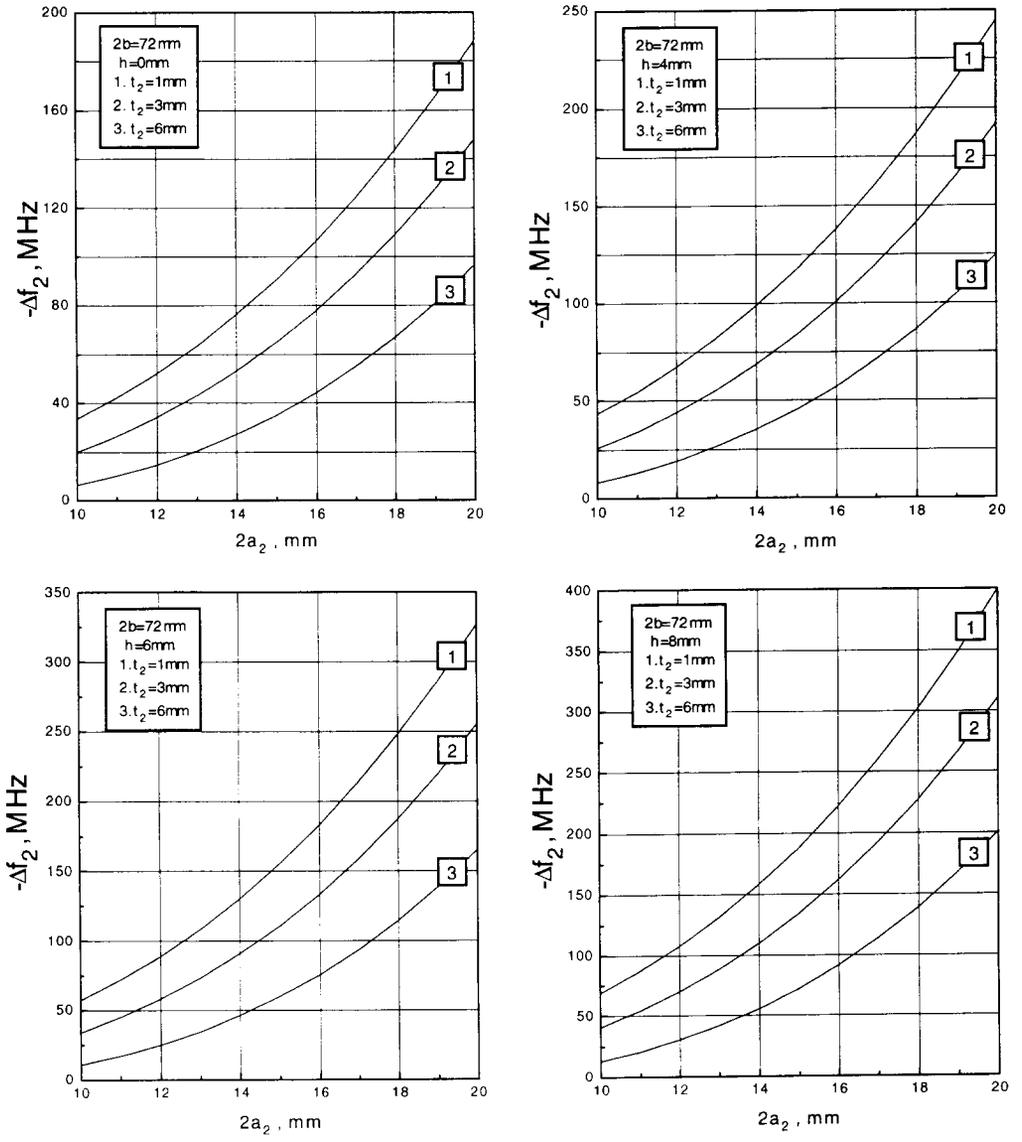

Fig. 10. Frequency shift of coupler cell because of two coupling window of WG2 with coupler cell with two drift tubes and round-type protrusion height h.

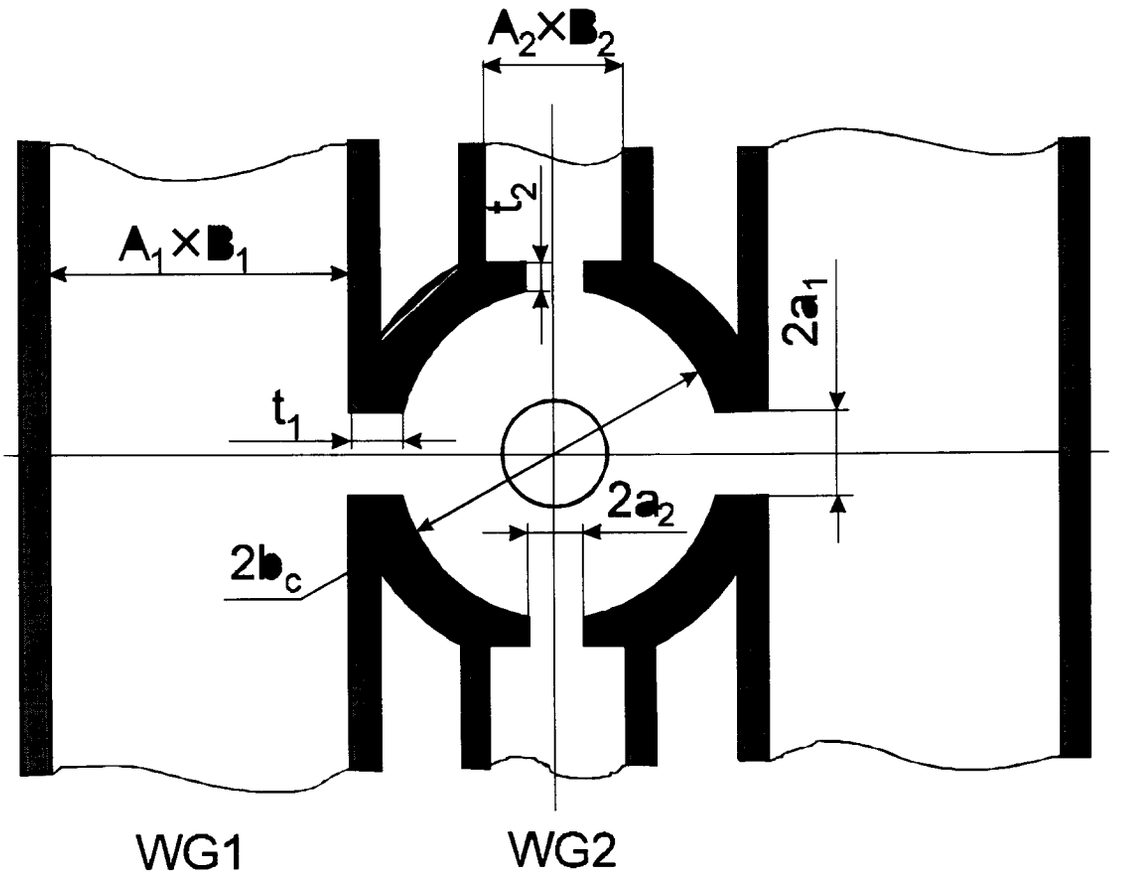

Fig 11 Cross-section of the coupler cell connected with rectangular waveguides.

4. Measurements of field distribution and Q-factor.

The perturbation method was used for measurements of the electric field longitudinal component distribution along DLW SBLC at frequencies of the first dipole mode (see Fig.6).

At the first stage the field distribution at the first dipole mode frequencies for the structure consisting of 30 initial cells of DLW SBLC with the coupler has been investigated. Dimensions of the coupler have been chosen earlier, taking into account only the requirements for E_{01} mode at f=2998 MHz . We did not expect satisfactory power withdrawal through the coupler at frequencies of the dipole mode. But the knowledge of E_z distribution for the case of the mismatched coupler at the hybrid wave is helpful for the correction of the field distribution over the initial part of DLW SBLC. The dimensions of the DLW were chosen so that the section has the constant gradient . The corresponding distribution are presented in Fig.12. Here the value proportional to the square root of the frequency shift and hence to the E_z component is taken as the ordinate. Some conclusions can be made on the basis of Fig.12. First, it is clear that higher modes are trapped in the constant gradient structure. The first trapped mode appears at the frequency of 4130 MHz and occupies five initial cells (Fig.12.a). There is no field in the coupler. The last trapped mode in the structure consisting of 30 cells appears at the frequency of 4161.6 MHz , the π-mode being monitored in the end 5-6 cells (Fig.12.c). At that frequency there also is practically no field in the coupler cell. Field distributions for the subsequent frequencies 4164.1 - 4216 MHz are shown in Fig.12. e,f,g,h,i,j. Here one can observe only the "tail" part of trapped modes because their "head" part (π-mode) should be situated beyond the 30-th cell. At frequencies 4164 - 4194 MHz the field penetrates into the coupler cell.

Starting from f=4185 MHz (Fig.12.d) the field in the first DLW cells decreases. It proves that the initial part of the structure traps the dipole modes and they don't penetrate into the coupler. Thus , the trapped higher modes have been coupled with the section input in the frequency band 4131 - 4194 MHz , the field being absent inside the coupler cell at f=4130 - 4150 MHz . At frequencies higher than 4150 MHz the field starts to penetrate into the coupler and its amplitude is comparable with that in the first cell at frequencies 4164 - 4194 MHz . Indirectly this fact indicates that the coupler cell eigen frequency for the E_{11} mode is situated in the range of 4164 - 4194 MHz.

Experiments on the study of field distribution in 30 cells of DLW at frequencies of the first dipole mode have shown that for the successful damping of that mode by means the coupler, a method should be developed to vary the coupler dipole mode frequency. At the same time the coupler eigen frequency at the fundamental mode should remain unchanged. The computation results presented in chapter 1 also indicate that there is a necessity to have definite values of the dipole mode frequency as well as the coupler Q-factor at those frequencies for the purpose of effective extraction of the hybrid mode power from the coupler. Unfortunately , till now, such a model failed to obtain relationships for the experimental determination of the coupler eigen parameters at the hybrid mode as it was done for the fundamental mode. In this connection the problem of coupler cell tuning becomes rather complicated.

Some experimental results permit the evaluation of the influence of the coupler cell 's eigen frequency on the electric field amplitude distribution in the DLW connected with the coupler. Through the beam aperture either a metal or dielectric plunger is inserted into the system. The dimensions of plunger were determined earlier for the case of the fundamental mode. The metal plunger was inserted into the coupler up to 5 mm depth whereas the dielectric one up to 15 mm. Since the plungers are positioned in the region of strong electric field for the E_{010} mode as well as for the E_{110} mode, it is natural to expect the coupler frequency to be decreased. Indeed, that frequency diminished by 10 MHz for the metal plunger and by 25 MHz for the dielectric one. That experimental values were obtained for the case of the coupler cavity connected with two rectangular waveguides and being excited through the butt-end wall.The electric field longitudinal component distributions along the DLW section measured at the distance 6 mm from the axis are presented in Fig.13. The distribution in Fig.13d corresponds to the case without plungers, Fig.13b - to the case with a metal plunger , Fig.13c - with dielectric plunger , Fig.13d,e - to the case with the dielectric plunger and displacement of the short-circuits in rectangular waveguides by $\pm$20 mm respectively. In these experiments two other ends of the rectangular guides are connected to the T-junction which can be considered as short-circuits at the dipole mode frequencies. If the short-circuits are removed from the coupling slot by 20 mm the field amplitude in the coupler increases. On the contrary if they are brought nearer to the coupling slot the field amplitude in the coupler increases. The strong dependence of the coupler field amplitude on the position of short-circuits indicates indirectly the good coupling between the coupler cell and rectangular waveguides. The loaded Q-factor value at minimal coupling with the structure, consisting of 30 cells DLW and the coupler, was about 10500 and

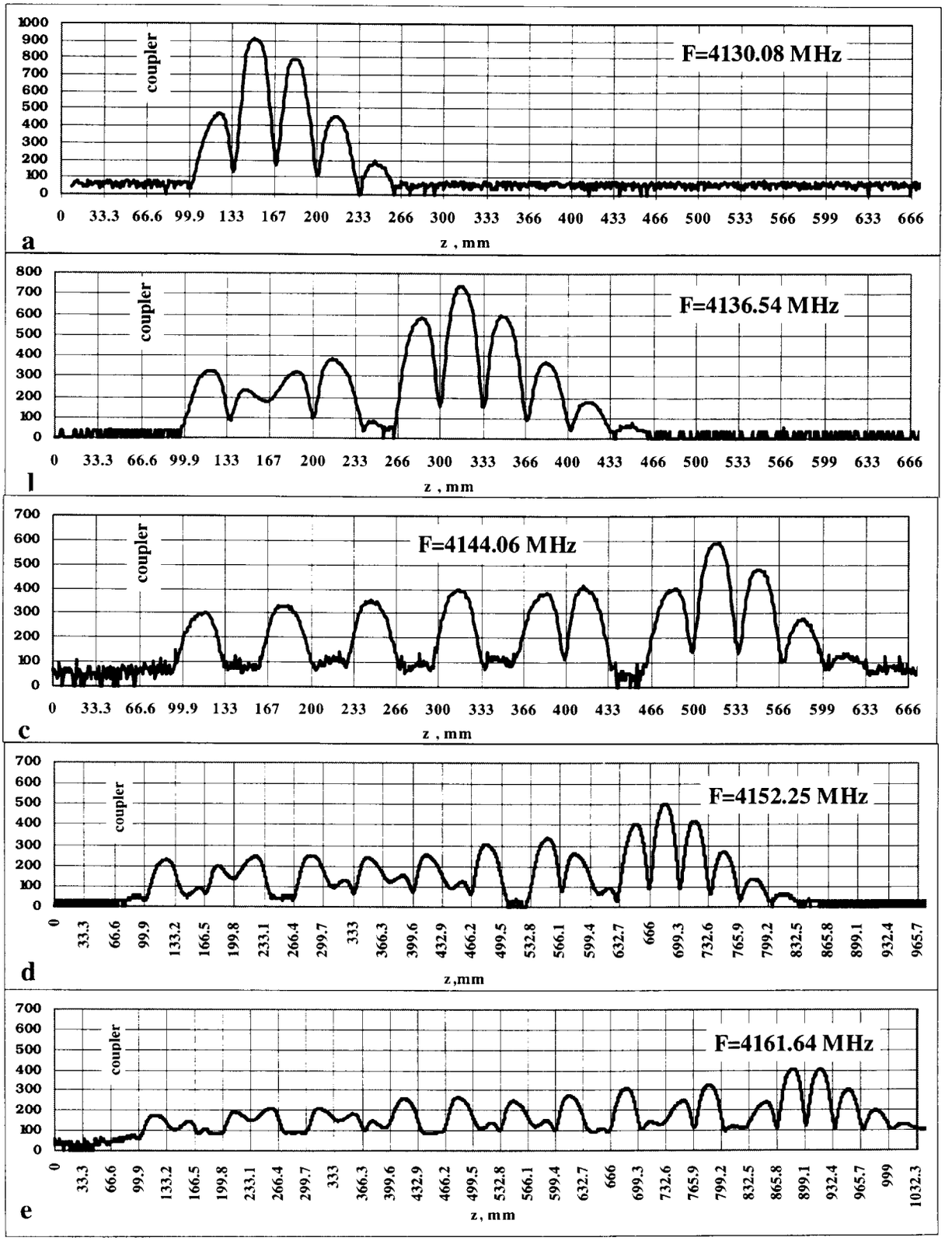

Fig. 12. The field distribution of 30 cells of SBLC DLW at trapped HOM at the first dipole frequency band.

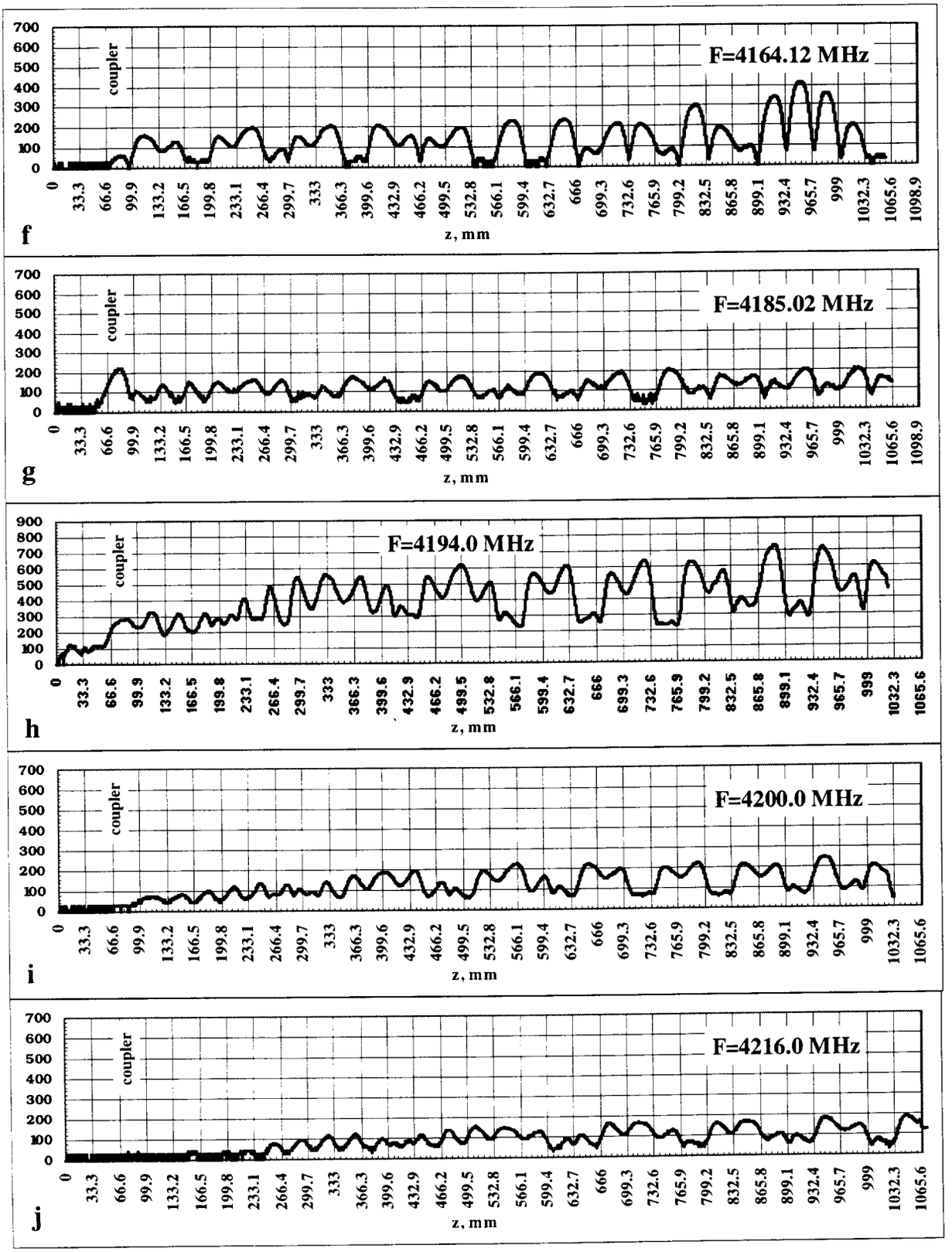

Fig. 12. The field distribution of 30 cells of SBLC DLW at trapped HOM at the first dipole frequency band.

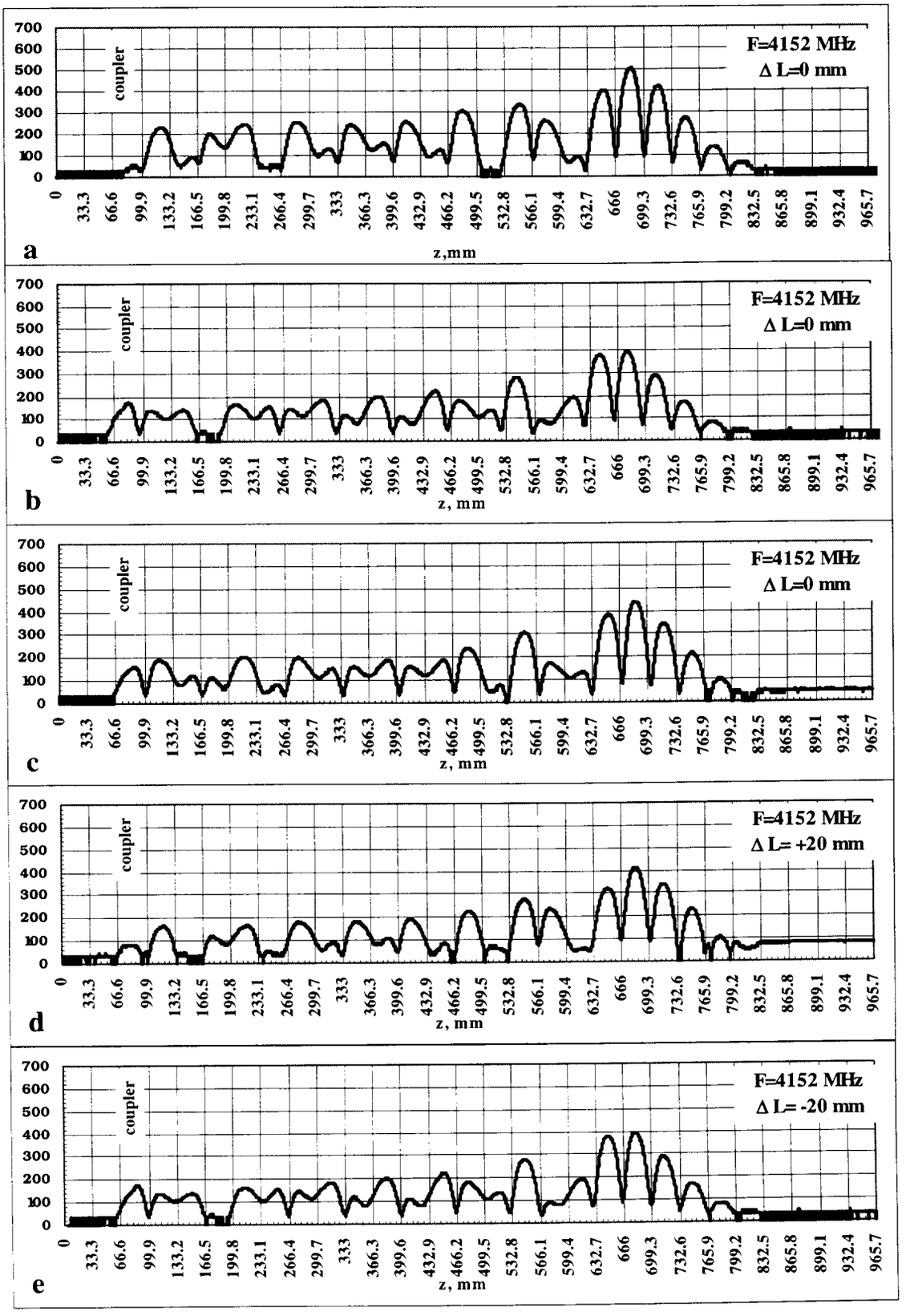

Fig. 13. :The field distribution of 30 cells of SBLC DLW at trapped HOM a-without tube in the coupler beam-pipe ; b -with copper tube in the coupler beam-pipe; c, d, e - with dielectric tube in the coupler beam-pipe

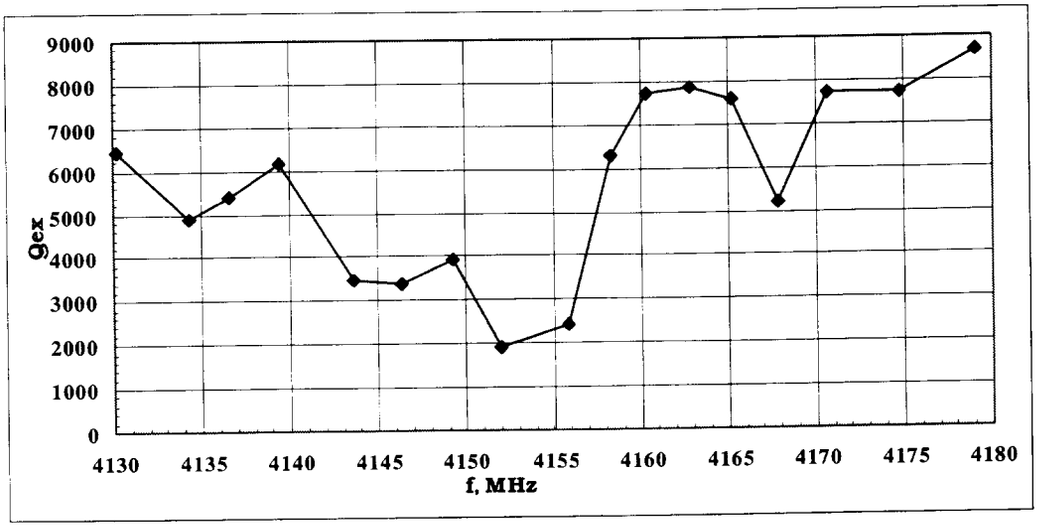

a)

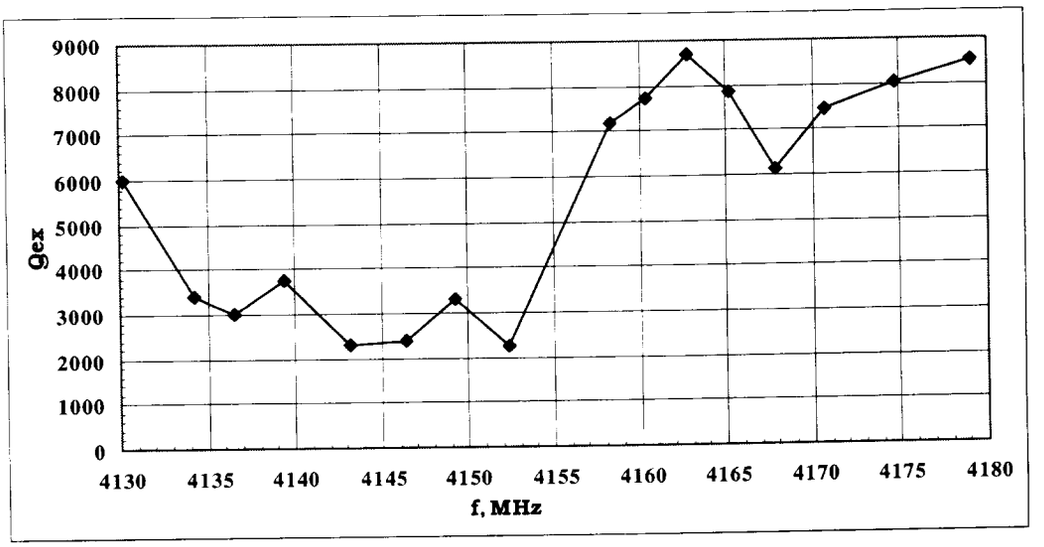

b)

Fig. 14. External Q-factor at the 30 cells SBLC DLW at trappered HOM versus frequency for cases at optimal tuning at frequencies 4152 MHz (a) and 4146 MHz (b).

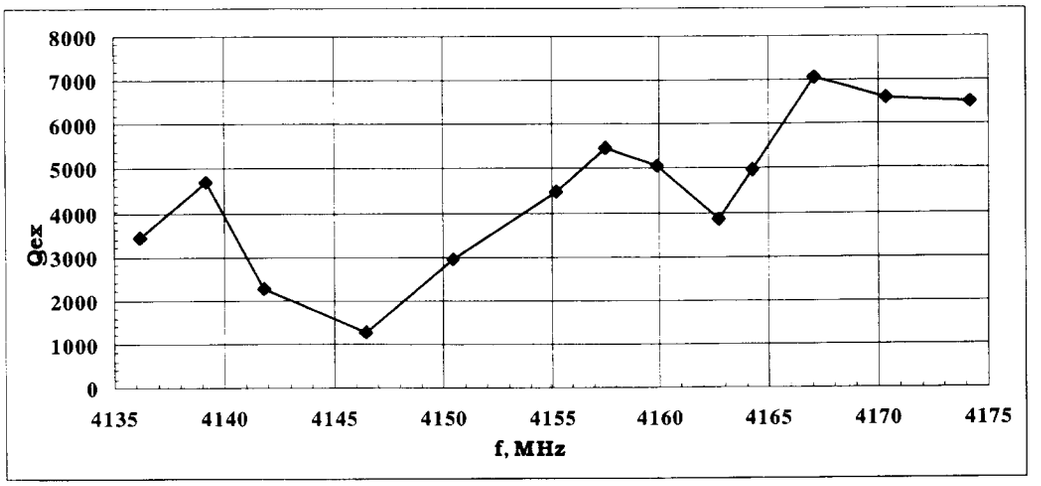

a)

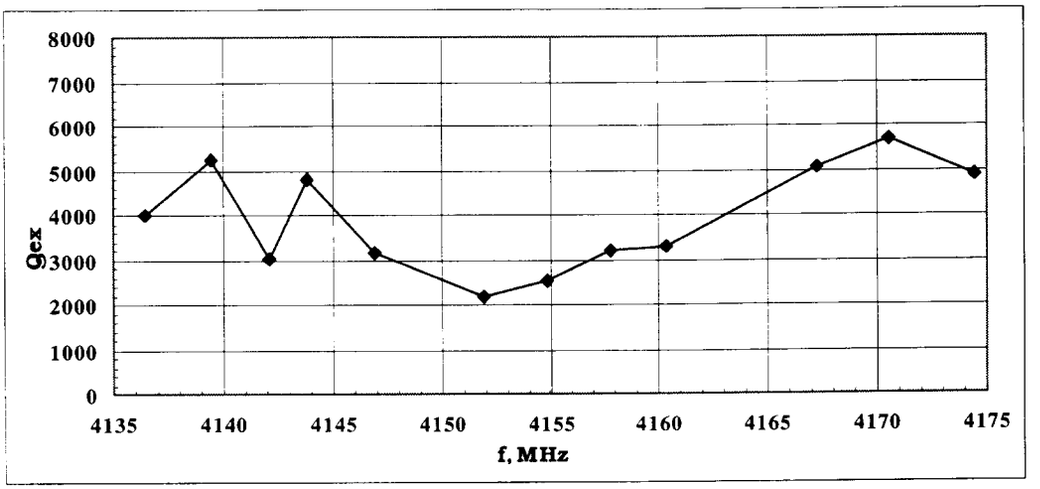

b)

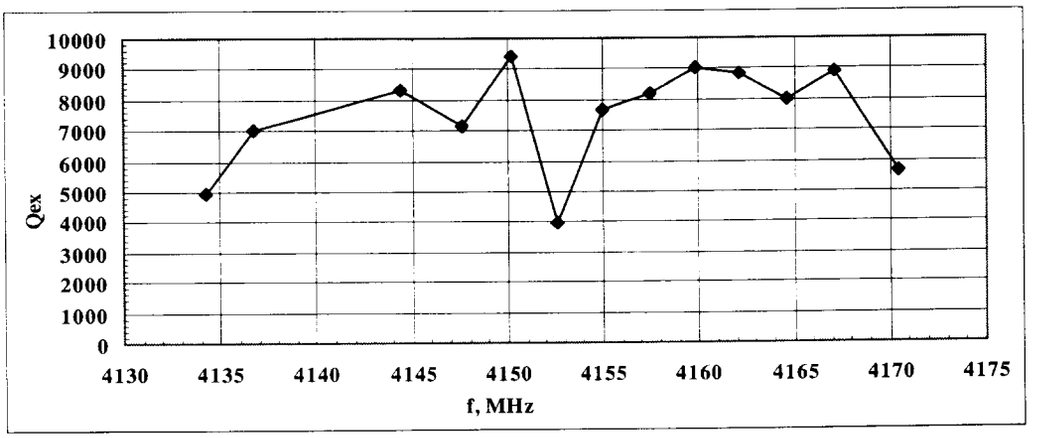

c)

Fig. 15. External Q-factor of the 30 cells DLW SBLC at trappered HOM versus frequency for the coupler with waveguides WG2 (a,b) and waveguides WG1 (c)

did not change with short-circuit replacement. To improve the reliability of the instrumentation the coupling value was increased which resulted in the loaded Q-factor decrease down to 8000 - 9000.At the next stage of investigations the short-circuiting plungers were replaced by waveguide sections with tuning pins (8 in Fig.6.) and matched loads (6 in Fig.6.). At a certain frequency of the first dipole mode the Q-factor of the structure, consisting of 30 cells DLW SBLC and the coupler, has been reduced by means of the tuning pins and the change of the distance between the short-circuits and T-junction. The latter is effected by the insertion into this junction a metal plane. Corresponding results are shown in Fig.14. . Here the minimal values of the loaded Q-factor are obtained at f=4152 MHz (Fig.14.a) and at f=4146 MHz (Fig.14.b). In these experiments the coupler frequency was reduced by 25 MHz by means of the dielectric plunger as was described above. Such possibility of decreasing the external Q-

factor by about 4 times at one frequency of the dipole mode band is

very promising. Results presented in our previous reports were related to the structure consisting of 10 DLW cells, so it appears to be not correct to compare those results with those obtained now.

In the working version of the system under consideration the dielectric plungers can be replaced by specific ring-type protrusions. It would be shown below that the coupler frequency could be decreased also by cutting two additional slots which would damp the other dipole mode with orthogonal polarization.

Fig.15. demonstrates possibilities of the second polarization hybrid wave damping through the waveguides, connected to the coupler cavity with their butt-ends (waveguides WG2 in Fig.11.). The coupler and waveguides to be experimentally studied had the following dimensions : $2b_c$=70mm, $2a_2$=20mm, t_2=4mm, A_2=48mm, B_2=24mm. The circular protrusion dimensions were : h_1=7mm, r_1=25mm, Δr_1=5mm. The obtained decrease in the external Q-factor value amounted to either 1200 (Fig.15a) or ≈2200 (Fig.15b) for broader frequency band depending on the value of mismatch introduced into connected waveguides by means of pins. It should be noted that with such dimensions of the coupler and circular protrusion we failed to obtain satisfactory results in the hybrid wave damping through waveguides connected to the coupler parallel to each other (waveguides WG1 in Fig.11, their dimensions being $2a_1$=35mm and t_1=10mm). The external Q-factor as a function of the frequency is presented in Fig.15 for one of admittance optimal values. The admittance was introduced into the rectangular waveguides with narrow cross-section.

5. Conclusion.

The capability of symmetric SBLC coupler to damp the fields of the first dipole mode was investigated. The requirements for the frequency and Q-factor of the hybrid coupler were obtained. Some approaches to the tuning of the coupler at the hybrid mode while maintaining the matching at the fundamental frequency were investigated. The field distribution of the 30 cell SBLC DLW at trapped HOM were measured. The Q-factor of the one meter SBLC DLW could be decreased by factor 5 for both polarization. The design for a hybrid coupler for the SBLC accelerating section is proposed.

Our studies have indicated there are no principal obstacles in the development of the coupler which provides damping of the first dipole mode in both polarization in the frequency band. At the same time there should be no reflections at the fundamental mode frequency. The changes in coupler construction could be insignificant.

6. References.

1. G.Romanov, S.Ivanov, M. Dohlus, N. Holtkamp, „ Some Remarks on the Location of Higher Order Modes in Tapered Accelerating Structure with the use of a Coupled Oscillator Model „, to be published in 1995 PAC proceedings, Dallas.

2. V. Kaljuzhny, N. Sobenin, M. Dohlus, N. Holtkamp et al. „ Design and Performance of a Symmetric High Power Coupler for a 6 Meter S-Band Linear Collider Accelerating Structure“ , Internal Report, DESY M 94-11, October, 1994.

3. N. Sobenin, B. Zverev, „ Electrodynamic Characteristics of Accelerating Resonators „ , Moscow, Energoatomizdat, 220 pages, 1993.